Tectonics

RESEARCH ARTICLE
10.1029/2018TC005163

Key Points:
- Analysis of seismicity in West Bohemia revealed an interaction of compressive fault steps producing stress anomaly with size of 300 × 300 m
- Breaking a barrier between faults produced anomalous focal mechanisms and a mainshock-aftershock sequence untypical for the swarm region
- Stress modeling confirmed rapid rotations of stress axes close to the fault tips and explained a wide variety of focal mechanisms observed

Supporting Information:
- Data Set S1
- Data Set S2
- Data Set S3
- Supporting Information S1

Correspondence to:
V. Vavryčuk,
vv@ig.cas.cz

Citation:
Vavryčuk, V., & Adamová, P. (2018). Detection of stress anomaly produced by interaction of compressive fault steps in the West Bohemia swarm region, Czech Republic. *Tectonics*, *37*, 4212–4225. https://doi.org/10.1029/2018TC005163

Received 30 MAY 2018
Accepted 17 OCT 2018
Accepted article online 24 OCT 2018
Published online 18 NOV 2018

Detection of Stress Anomaly Produced by Interaction of Compressive Fault Steps in the West Bohemia Swarm Region, Czech Republic

Václav Vavryčuk[1] **and Petra Adamová**[1]

[1]Institute of Geophysics, The Czech Academy of Sciences, Praha, Czech Republic

Abstract Observations of the 2008–2014 seismic activity in West Bohemia, Czech Republic, provide evidence of interaction of compressive fault steps that created local stress anomaly and triggered a seismic sequence with exceptional properties. The West Bohemia is a geothermal area, characterized by persistent fluid-driven seismicity in the form of earthquake swarms. The focal zone is formed by two weak and fluid-eroded parallel strike-slip faults with a step of about 200 m. The fault segments were activated successively by the 2008 and 2011 swarms with magnitudes of the strongest events of 3.8 and 3.7, respectively. In 2014, a fracture linking both segments was formed or activated by a mainshock-aftershock sequence. The aftershock decay was very fast, and the focal mechanism of the strongest event with magnitude of 4.2 was inconsistent with the regional background stress. The stress inversion of 957 focal mechanisms revealed a stress anomaly characterized by interchanging the σ_2 and σ_3 principal stress axes in the area of fault interaction. The modeling of the Coulomb stress change confirmed that the stress anomaly could completely disturb the regional background stress and produce the rotation of the principal stress axes retrieved from focal mechanisms. The faults activated or newly formed within the compressive stress anomaly were of high strength, which caused the anomalous mainshock-aftershock character of the 2014 activity and the rapid aftershock decay. Linking the two previously active isolated faults during the 2014 activity increased the expected moment magnitude M_w of a possible strongest earthquake from 5.0 to 5.4.

1. Introduction

Faults in seismically active areas form complex systems. They can be of irregular shapes either smoothly bent or displaying kinks; they can mutually intersect or form systems of discontinuous parallel fault segments called fault stepovers or simply fault steps (Fossen & Rotevatn, 2016; Micklethwaite et al., 2015). The closely spaced fault steps, fault tips, and fault irregularities produce damage zones (Kim et al., 2004), complexities in stress pattern (Arrias et al., 2011; Crider & Pollard, 1998; Lin & Stein, 2004; Madden et al., 2013), and complexities in characteristics of seismicity and in wavefields radiated by earthquakes (Adda-Bedia & Madariaga, 2008; Madariaga et al., 2006).

Since parallel active faults occur widely in nature, their behavior has been studied with a particular attention: using in situ observations (Wesnousky, 2006; Zuza et al., 2017) as well as modeled numerically (Crider & Pollard, 1998; Gupta & Scholz, 2000; Harris & Day, 1993, 1999) or in the lab (Mansfeld & Cartwright, 2001; Sagong & Bobet, 2002; Špičák & Lokajíček, 1986; Yang et al., 2014). The faults interact if being close enough with separation distance d roughly scaled as $d \leq 0.1\ L$, where L is the individual fault length (An, 1997). The fault steps can be compressional or dilatational depending on whether they produce compressional or dilatational stress anomaly between the fault segments. The two types of fault steps are bound with a different character of faulting (reverse or normal) and different stress drops and also behave differently for rupture jumping between the two fault segments (Nevitt & Pollard, 2017; Oglesby, 2008; Ryan & Oglesby, 2014). Obviously, a possible linkage of the stepovers or rupture jump between the fault segments has important consequences for seismic hazard.

In this paper, we analyze interactions of faults from observations of a seismic activity in West Bohemia, Czech Republic. The studied data set is quite unique, because the focal zone is formed by two parallel fault segments characterized by abundant seismicity recorded by a dense network of seismic stations. Accurate double-difference locations of earthquakes (Bouchaala et al., 2013; Fischer et al., 2014; Hainzl et al., 2016) and their focal mechanisms (Vavryčuk, 2011; Vavryčuk et al., 2013, 2017) make possible tracing spatial

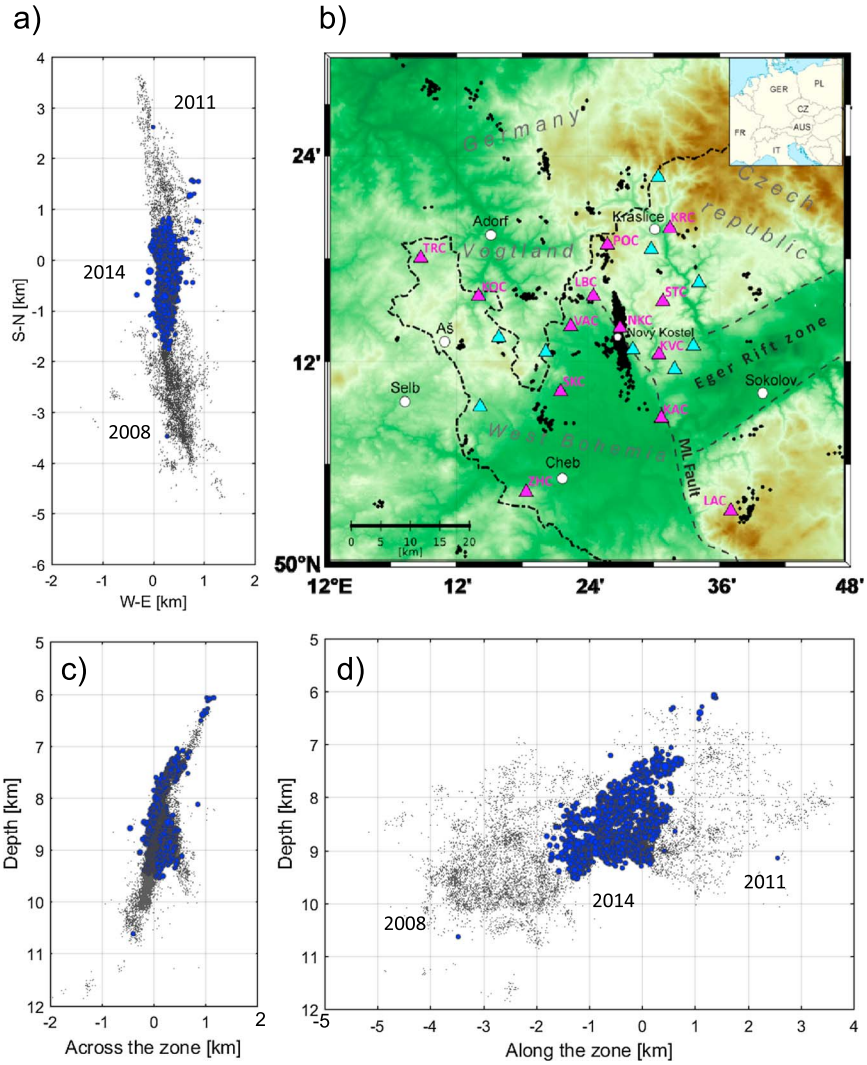

Figure 1. Map of the seismically active area in the West Bohemia region. The locations of earthquakes with ML ≥ 0.5 that occurred in the period of 1995–2014 (black dots) are shown in the map view (a, b) and in the vertical sections across the fault zone (c) and along the fault zone (d). The triangles in Figure 1b show the positions of the West Bohemia Network (WEBNET) stations: magenta triangles, online stations; cyan triangles, offline stations. The blue dots in Figures 1a, 1c, and 1d denote the locations of earthquakes in the 2014 earthquake sequence. ML fault = Mariánské-Lázně fault. The earthquake locations were computed using the hypoDD method.

variations of stress and identifying a stress anomaly originated from interaction of the fault segments. The observed variation of stress due to the fault interaction is verified by modeling of the Coulomb stress change, and a possible role of fluids in linkage of the fault segments is discussed.

2. The 2008–2014 Seismic Activity in West Bohemia

2.1. Tectonic Setting

The West Bohemia region is a geodynamically active area situated in the western part of the Bohemian massif with a persistent seismic activity characterized by a frequent occurrence of earthquake swarms. The most prominent earthquake swarms occurred in 1985/1986, 1994, 1997, 2000, 2008, 2011, and 2014 (Čermáková & Horálek, 2015; Fischer et al., 2010, 2014; Jakoubková et al., 2017; Vavryčuk, 1993) at the same epicentral area called the Nový Kostel focal zone (Figure 1). The isolated earthquakes as well as earthquake swarms occur also in other areas, but they are weaker and less frequent (Fischer et al., 2014). The earthquake swarms last

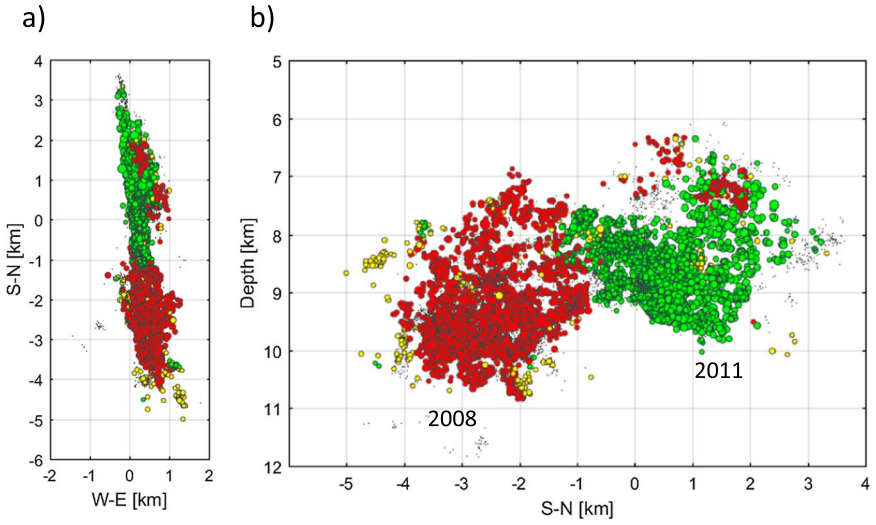

Figure 2. Locations of earthquakes with $M_L \geq 0.5$ that occurred in the period from 2008 to 2011 are shown in the map view (a) and in the vertical section along the fault (b). Red circles, the 2008 swarm earthquakes; green circles, the 2011 swarm earthquakes; yellow circles, the earthquakes between the swarms.

typically from several days to several months, and the activity is focused at depths from 6 to 12 km. The strongest instrumentally recorded earthquake was the M_L 4.6 earthquake on 21 December 1985.

Active tectonics in the area is related to Tertiary and Quaternary volcanism manifested by CO_2 emanations and mineral springs. The wet and dry mofettes occur in several degassing sites along the main tectonic fault zones (Braeuer et al., 2018, 2009; Hrubcová et al., 2017; Kaempf et al., 2013). The tectonic structure of the area is characterized by two main fault systems: the (pre-Neogen) Mariánské Lázně NW-SE fault system and the Ore-Mountain WSW-ENE fault system related to Tertiary Eger Rift opening. A recently most active fault is the left-lateral strike-slip fault in the N-S direction, which forms the eastern boundary of the Cheb Basin filled by Tertiary and Quaternary sediments up to 300-m thick. Another active fault is the right-lateral strike-slip fault in the WNW direction. The seismically active faults were identified at depth by foci clustering and focal mechanisms (Vavryčuk et al., 2013), and also have some geological evidence on the surface (Bankwitz et al., 2003).

2.2. Seismic Activity in 2008–2014

The seismic activity is monitored by local three-component West Bohemia Network (WEBNET) seismic stations (Figure 1). The network was operating since 1994, and the number of stations gradually increased (Fischer et al., 2014). Since 2008, the network is composed of 22 local three-component short-period stations having epicentral distance smaller than 25 km and covering the area uniformly with no significant azimuthal gaps. The sampling frequency is 250 Hz, and the frequency response is flat at least between 1 and 60 Hz. The station with the nearest epicentral distance (station NKC) is additionally equipped with a broadband STS-2 seismometer. The detection threshold magnitude of the WEBNET network is less than −0.5, and the magnitude of completeness of the earthquake catalog estimated from the magnitude-frequency distribution is about −0.3 (see Fischer et al., 2010, their Figure 4).

Three prominent earthquake sequences occurred in West Bohemia during the period of 2008–2014: two earthquake swarms in 2008 and 2011, and a mainshock-aftershock sequence in 2014 (Figures 2 and 3). The 2008 earthquake swarm lasted 3 months and involved more than 25,000 events with magnitudes M_L up to 3.8. It activated a southern segment of the focal zone (Figures 2 and 3a). The 2011 earthquake swarm lasted about 2 months, but most of the energy was released in the first 3 weeks and involved more than 23,000 events with magnitudes M_L up to 3.7. The swarm activated a northern segment (Figures 2 and 3b). The seismic activity in 2014 lasted about 3 months and consisted of three phases with large gaps between them and with M_L of the strongest events 3.5, 4.2, and 3.6. The sequence involved about 6,700 events with foci concentrated at the conjunction of the southern and northern segments of the focal zone activated

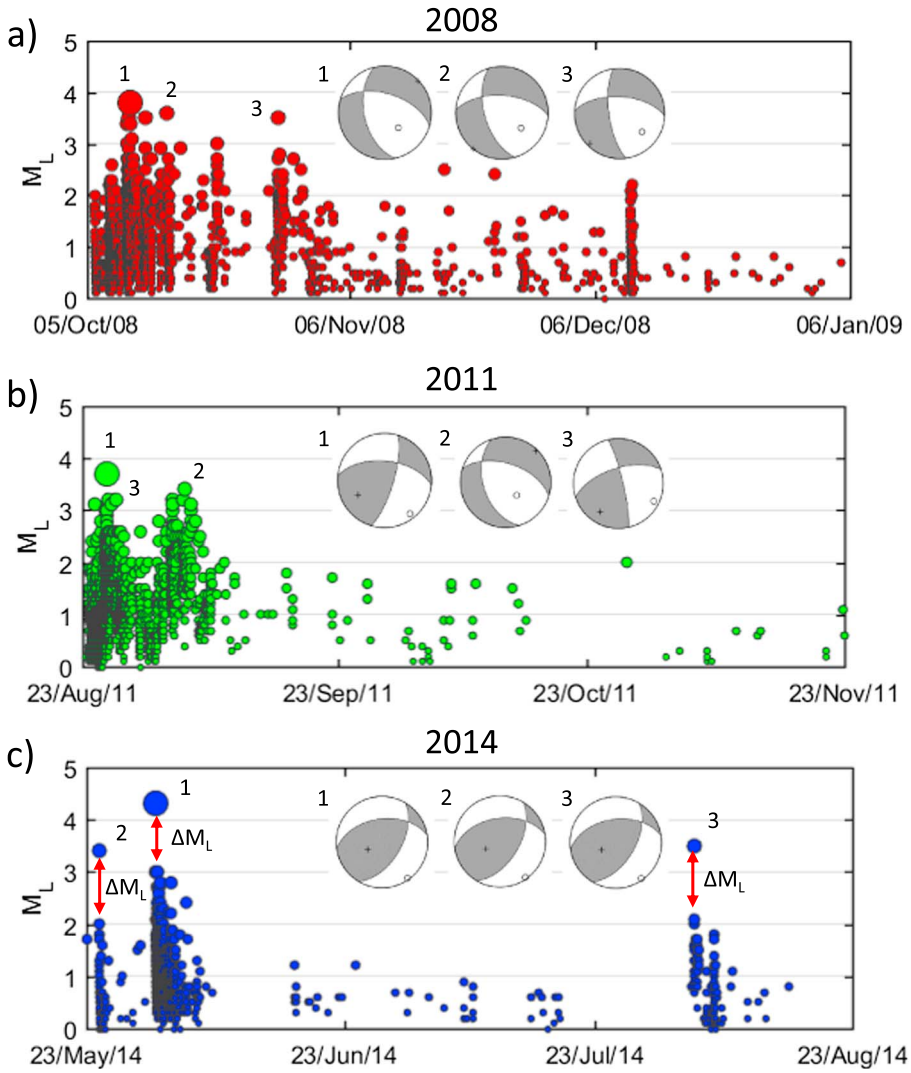

Figure 3. Magnitude-time plots of the 2008 (a), 2011 (b), and 2014 (c) seismic sequences together with focal mechanisms of three strongest earthquakes in each sequence. M_L = local magnitude. Magnitude difference ΔM_L greater than 1 between the strongest and second strongest events in the three phases of the 2014 activity (red arrows in Figure 3c) indicate the mainshock-aftershock character of the sequence. Such gaps are missing in the 2008 and 2011 seismic sequences.

during previous swarms (Figure 1). As seen from Figure 3c, the 2014 activity is exceptional. The magnitude difference ΔM_L between the strongest and the second strongest event in each phase is much higher than that in the previous swarms. The difference attains a value of $\Delta M_L \sim 1$ pointing to a standard mainshock-aftershock sequence rather than to an earthquake swarm (Jakoubková et al., 2017).

2.3. Decay of Aftershocks in 2008–2014 Sequences

Except for an anomalously high value of ΔM_L (see Figure 3c), also the character and duration of the seismic energy release was different during the 2014 sequence compared to the 2008 and 2011 earthquake swarms. The three seismic sequences consisted of several phases of intense activity and duration, and decay of aftershocks of individual phases were distinctly different. Jakoubková et al. (2017, their Figure 5b) reported that the 2014 sequence was characterized by a fast energy release compared to the previous sequences. This can be illustrated by calculating the event rate as a function of time for the studied sequences. A convenient way is to calculate the number of events that occurred in a seismic sequence within a moving time window (e.g., several hours). The obtained time-dependent rate curve displays several maxima reflecting each phase of an intense activity within the sequence. Subsequently, sorting the rates in the descending order yields the

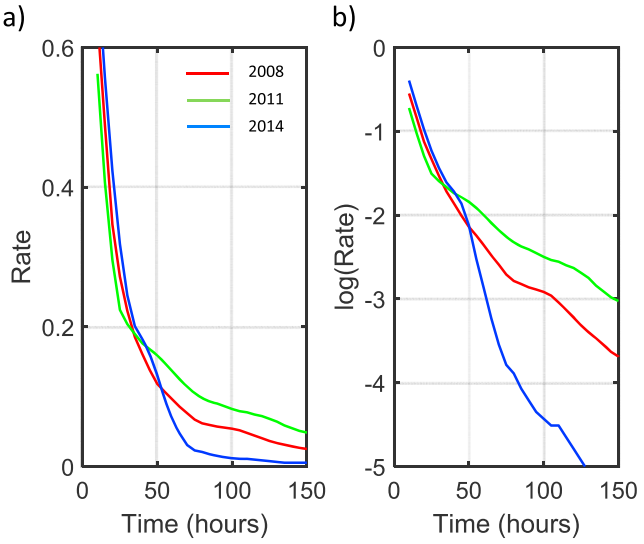

Figure 4. Normalized event rate sorted according to the activity level. The event rate is shown in the linear (a) and logarithmic (b) scales. The event rate is calculated as the number of events with the local magnitude $M_L > 0.5$ that occurred in the moving time window of 5 hr. The event rates are sorted in the descending order and normalized to their maximum. The timescale shows 30 time intervals covering in total of 150 hr.

activity decay in time averaged over the individual activity phases. As shown in Figure 4, the activity decay is similar for all three sequences for the first 2 days. After that, the activity in 2014 decreases significantly faster than in 2008 and 2011.

2.4. High-Resolution Image of the Focal Zone

Accurate double-difference locations of the 2008, 2011, and 2014 events reveal that geometry of the focal zone is complex (Vavryčuk et al., 2013). The main active fault has a strike of 170°. Its dip is about 65° at depths above 8 km (Figure 1c), but the fault is bent at 8 km and continues more steeply to greater depths with a dip of 80°. Apart from the main active fault, few minor fault segments with strike and dip of 305° and 65° cross the focal zone being well visible in the vertical cross section (Figure 1c).

Interestingly, the southern and northern segments of the main fault with strike of 170° (Figure 5a) do not form a single fault plane but they are actually fault stepovers—two parallel fault segments that are offset from each other at depth between 8 and 9 km. The step width is about 200 m, and the overlap between the segments is of the same size or less. This area was particularly activated during the 2014 seismic sequence (Figures 5b and 5c).

3. Focal Mechanisms

Focal mechanisms of the 2008 swarm earthquakes were calculated by Vavryčuk and Hrubcová (2017) using the moment tensor inversion of amplitudes of direct *P* waves. The selected 483 swarm earthquakes with magnitudes ranging from 1.0 to 3.8 recorded at the WEBNET seismic network were located with high precision by Bouchaala et al. (2013) using the HypoDD method. Accurate station amplifications, which included local site effects, were determined using the network calibration (Davi & Vavryčuk, 2012). The velocity records were integrated into displacement and band-pass filtered in the frequency range of 1–25 Hz in order to suppress seismic noise. The amplitudes of the direct *P* wave were

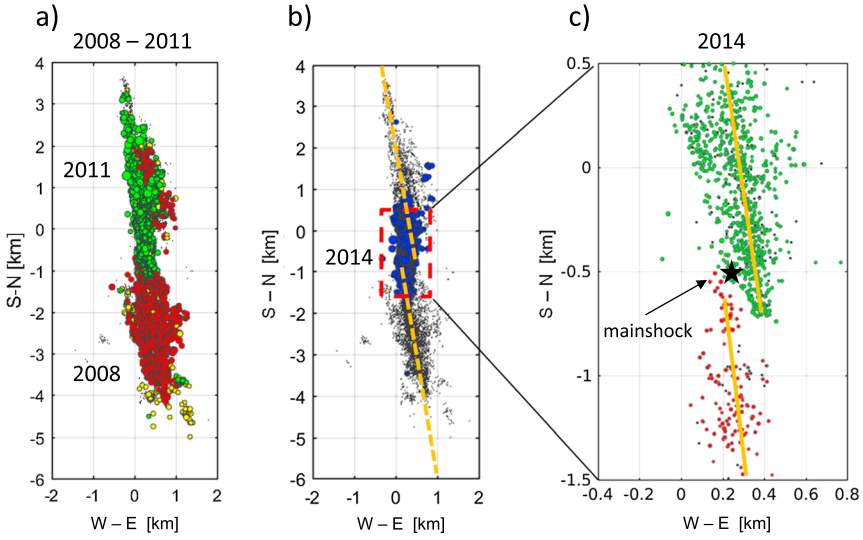

Figure 5. Locations of earthquakes with ML ≥ 0.5 that occurred during the 2008, 2011, and 2014 sequences shown in the map view. (a) Red circles, the 2008 earthquakes; green circles, the 2011 earthquakes; yellow circles, earthquakes occurring between the 2008 and 2011 swarms. (b) Blue circles, the 2014 earthquakes; black dots, the 2008 and 2011 earthquakes. (c) A zoomed view of the 2014 seismic activity. Red circles, the 2014 earthquakes occurring on the southern fault segment; green circles, the 2014 earthquakes occurring on the northern fault segment. Yellow full/dashed lines in Figures 5b and 5c show the fault steps.

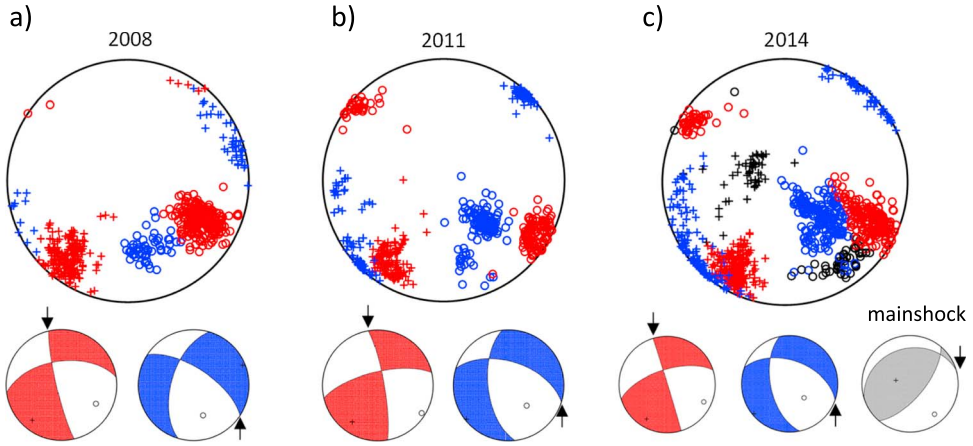

Figure 6. The *P*/*T* axes and centroid focal mechanisms of (a) 246 earthquakes in 2008, (b) 261 earthquakes in 2011, and (c) 450 earthquakes in 2014. The *P* and *T* axes are marked by the circles and the plus signs, respectively. The beach balls show the characteristic strike-slip focal mechanism associated with the fault steps (red), the oblique normal focal mechanism associated with the conjugate minor fault segments (blue), and the anomalous reverse focal mechanism associated with the fracture that linked the fault steps (gray). The black arrows mark the fault plane determined by the fault instability criterion (Vavryčuk, 2014).

inverted for full moment tensors using the generalized linear inversion and decomposed into the double-couple (DC) and nondouble-couple (non-DC) components. The Green's functions were computed for a 1-D gradient velocity model using the ray method.

Focal mechanisms of the 2011 and 2014 seismic sequences were calculated using the moment tensor inversion developed by Vavryčuk et al. (2017). In this method, the principal component analysis is applied to *P* waveforms recorded at stations for finding the common wavelet representing the time derivative of the source-time function radiated by the source. The coefficients of the first principal component served as effective *P* wave amplitudes inverted for the moment tensor. The method is less sensitive to noise in data and more robust than the standard amplitude inversion. Vavryčuk et al. (2017) calculated moment tensors of 833 earthquakes of the 2014 seismic activity. In this paper, we additionally inverted for moment tensors of 316 earthquakes of the 2011 swarm in order to cover the whole period of activity between 2008 and 2014.

All focal mechanisms were checked for their quality. Based on the root-mean-square residuals (less than 0.3) and error limits of the *P* and *T* axes (less than 5°), we selected 246, 261, and 450 earthquakes with the most accurate focal mechanisms of the 2008, 2011, and 2014 sequences, respectively. As seen in Figure 6, the *P*/*T* axes of the focal mechanisms are clustered. They form two clusters in 2008 and 2011 but three clusters in 2014. The families of similar focal mechanisms were used for calculating the centroid focal mechanisms by applying the *k* means clustering (for details, see Vavryčuk et al., 2017).

The *P*/*T* axes in 2008 and 2011 form the so-called *butterfly wings* (Vavryčuk, 2011). The *P* wings (*T* wings) are defined by the *P* axes (*T* axes) of two families of focal mechanisms corresponding to two activated conjugate fault systems symmetrically oriented with respect to the maximum compression in the region. The activated faults are optimally oriented for shearing under the present-day stress field deviating from the maximum compression by about 30°. This is expressed by high fault instability based on the Coulomb failure criterion concept (Vavryčuk, 2011, his equation 2; Vavryčuk, 2014, his equation 13). The fault instability depends on the fault orientation in the given stress field. It can range from 0 (stable faults) to 1 (most unstable faults) and measures the susceptibility of faults to be activated. The two basic types of the focal mechanisms of the 2008 and 2011 swarms are (1) the strike slip with a weak normal or reverse component (Figures 6a and 6b, red beach balls) and (2) the oblique normal mechanism (Figures 6a and 6b, blue beach balls). The fault instability is close to 1 for both mechanisms. The strike-slip mechanism is associated with the fault steps (Figure 5) and represents the most typical mechanism in the region. The oblique normal mechanism is associated with small fractures also present in the focal zone being detected by high-resolution fault imaging using interpolation of accurate foci (Vavryčuk et al., 2013). No other distinctly different and statistically significant focal mechanisms have been detected in both swarms.

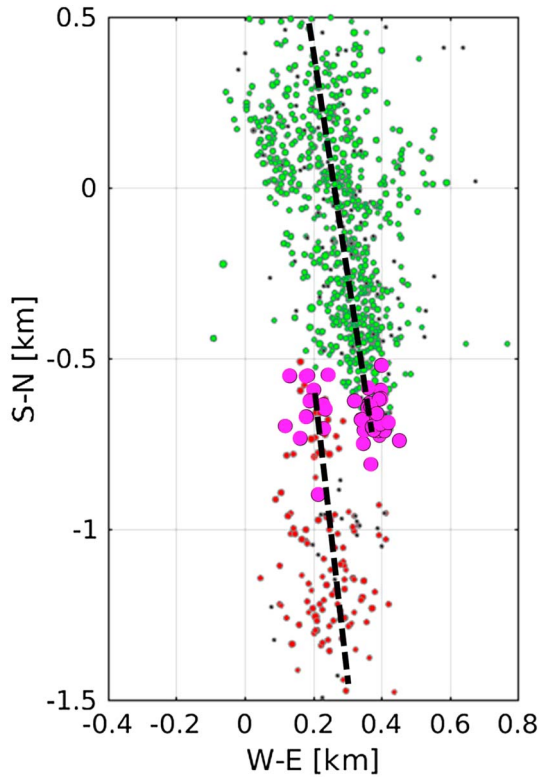

Figure 7. Locations of earthquakes of the 2014 sequence in the map view. Red small circles, earthquakes occurring on the southern fault segment; green small circles, earthquakes occurring on the northern fault segment. Magenta circles, earthquakes with the reverse focal mechanism. The black dashed lines show the fault steps. The threshold magnitude is M_L = 0.5.

By contrast, the 2014 earthquake sequence is different. Except for the mentioned two basic types of the focal mechanisms typical for the 2008 and 2011 swarms, another family of oblique reverse focal mechanisms appeared in 2014 (Figure 6c). The earthquakes of this family include the strongest events of the 2014 sequence (Figure 3c), and their *T* axes form a cluster close to the vertical axis (Figure 6c, black plus signs in the upper plot). Such positions of the *T* axes are inconsistent with the stress field reported for previous swarm activities in this focal zone (Vavryčuk, 2002, 2014). Hence, the anomalous reverse focal mechanisms and a non-swarm character of the 2014 sequence (Hainzl et al., 2016; Jakoubková et al., 2017) indicate a possible change of physical properties of the focal zone and might point to the formation of a local stress/strength heterogeneity in the focal zone, which affected the 2014 activity. A possible role of the fault interaction between the northern and southern segments is indicated by locations of earthquakes with reverse focal mechanisms, which concentrated near the tips of the fault segments (Figure 7, magenta circles).

4. Tectonic Stress

In order to analyze tectonic stress in the focal zone we use the public-open Matlab code STRESSINVERSE (http://www.ig.cas.cz/stress-inverse) for a joint inversion of focal mechanisms for stress and fault orientations developed by Vavryčuk (2014). The method is based on the Michael's inversion for stress (Michael, 1984, 1987) that is run in iterations and utilizes the fault instability criterion (Martínez-Garzón et al., 2016; Vavryčuk et al., 2013) for discriminating which of two nodal planes is the fault plane. The method is fast and robust and provides uncertainty limits of results.

The stress inversion applied to the 246 and 261 most accurate focal mechanisms of the 2008 and 2011 swarms indicates that the tectonic stress in the focal zone is quite stable during this time period with only insignificant changes in the principal stress directions (see Table 1 and Figure 8). The azimuth and plunge of the σ_1 axis is 125–135° and 30–35°, respectively. The σ_3 axis is nearly horizontal with azimuth of 220–230°. These directions were obtained also for a previous seismicity and are consistent with the regional background stress in the area (Vavryčuk, 2002). Slight changes between stress axes for the 2008 and 2011 swarms are probably connected to migration of foci because the swarms activated two differently located (southern and northern) fault segments (Figure 5a). Similar directions of the principal stress axes are also obtained when inverting a set of 400 focal mechanisms of the 2014 sequence consistent with those that occurred during the 2008 and 2011 swarms (Table 1, data set 2014a). By contrast, the stress inversion of the remaining 50 anomalous reverse focal mechanisms (Table 1, data set 2014b; Figure 7, magenta circles) yields quite different results (Figure 8). The σ_2 and σ_3 axes are switched, and the σ_3 axis is slightly rotated clockwise by about 15°. Since the positions

Table 1
Principal Stress Axes of the 2008, 2011, and 2014 Earthquake Sequences

Data set	Number of events	σ_1 axis		σ_2 axis		σ_3 axis	
		Az (°)	Pl (°)	Az (°)	Pl (°)	Az (°)	Pl (°)
2008	246	135.9 ± 0.7	35.3 ± 0.6	337.1 ± 2.0	52.8 ± 0.4	233.3 ± 0.8	10.2 ± 0.9
2011	261	125.8 ± 0.8	30.3 ± 1.1	323.0 ± 1.6	58.6 ± 1.1	220.3 ± 0.6	7.7 ± 0.8
2014a	400	124.7 ± 0.5	38.0 ± 0.5	318.7 ± 0.8	51.1 ± 0.5	220.1 ± 0.4	6.9 ± 0.4
2014b	50	142.2 ± 1.4	22.5 ± 1.5	47.0 ± 1.7	12.4 ± 1.5	290.2 ± 4.7	64.0 ± 1.5

Note. Az = azimuth; Pl = plunge; data set 2014a = the 2014 data set excluding the reverse focal mechanisms; data set 2014b = the 2014 data set of the reverse focal mechanisms.

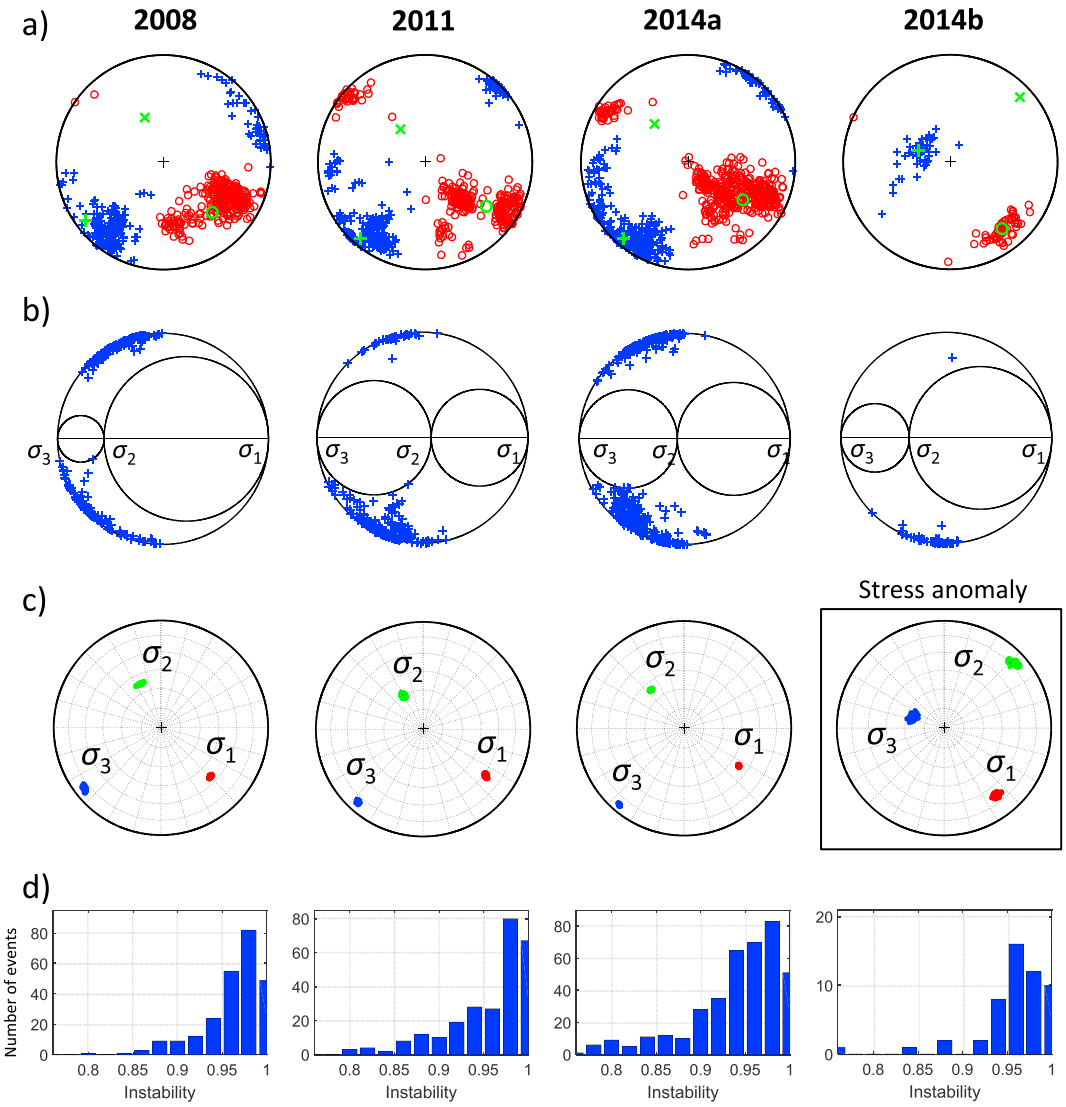

Figure 8. The *P*/*T* axes (a), Mohr's circles (b), principal stress axes (c), and histograms of the fault instability (d) for the 2008, 2011, and 2014 sequences. The earthquakes of the 2014 sequence are divided into two families: 2014a, earthquakes where the reverse focal mechanisms are excluded; 2014b, earthquakes of the reverse focal mechanisms. The red circles and blue plus signs in Figure 8a mark the *P* and *T* axes, respectively. The blue plus signs in the two half-planes of the Mohr's circles in Figure 8b discriminate faults symmetrically oriented with respect to the maximum compression. The histograms of the fault instability in Figure 8d indicate that the activated fault planes are well oriented for shearing under the given stress field.

of fault planes in the Mohr circle diagrams in Figure 8b lie in the area of expected validity of the Mohr-Coulomb failure criterion (Vavryčuk, 2011, his Figure 1), the fault planes are well oriented for shearing under the given stress fields. This is supported by values of the fault instability close to 1 (Figure 8d). The locations of faults in the upper/lower half-plane of the Mohr diagram discriminate which of the nodal planes are likely the fault planes (black arrows in beach balls in Figure 6).

5. Modeling of Fault Interaction in the 2014 Sequence

In order to verify that the fault interaction can significantly change the background stress field and produce anomalous focal mechanisms in the 2014 sequence inconsistent with regional stress, we modeled the static stress and the Coulomb stress change in the focal zone using the public-open Matlab code COULOMB 3.3 (https://earthquake.usgs.gov/research/software/coulomb/), see Lin and Stein (2004) and Toda et al. (2005). The code is based on formulae of Okada (1992) and calculates static displacements, strain, and stress

caused by slip along a fault or fault systems situated in an elastic homogeneous isotropic half-space. The Coulomb stress change has been modeled also by other authors for studying fault interactions on various scales (Fan & Shearer, 2016; Marzocchi & Melini, 2014; Turner et al., 2013). Such studies confirmed that the static stress change associated with large earthquakes can alter the principal stress orientations near the fault, which was frequently observed when compared stress inverted from focal mechanisms before and after large earthquakes (Hasegawa et al., 2012; Yoshida et al., 2012, 2014). Some studies are even able to map a detailed spatial distribution of principal stress orientations for the premainshock and postmainshock periods and correlate them with the static stress change (Yoshida et al., 2015).

We computed the static stress change for the fault steps simulating real geometry of the southern and northern fault segments in Figure 5. The step width is 200 m, and the sizes and orientations of both fault segments are the same. The top and bottom depths are 7 and 9.5 km, and the length and width are 3 and 2.6 km, respectively. The strike, dip, and rake angles characteristic for the focal zone are 169°, 74°, and −44°, respectively (Vavryčuk et al., 2013, their Figure 2). The friction coefficient on the faults is 0.55 being obtained by analyzing orientations of activated fractures in the focal area (see Vavryčuk, 2011). We calculate the static stress change produced by earthquakes occurred on both fault segments during the 2008 and 2011 swarms. The cumulative scalar moment of both swarms is assumed to be $M_w = 5.4$, which corresponds to cumulative slip of 35 cm. This value is slightly higher than that produced just by the seismic activity ($M_w = 5.0$) and reflects also the aseismic slip. For calculating the complete stress field around the fault steps, the principal stress axes of the background stress are identified with those obtained for the 2011 swarm (Table 1). The vertical stress gradients for the maximum, intermediate, and minimum stresses are 40, 24, and 20 MPa/km being derived from absolute stresses 320, 190, and 160 MPa at depth of 8 km reported by Vavryčuk (2002). The Young's modulus and the Poisson's ratio needed in the modeling are 8×10^4 MPa and 0.22. The Poisson's ratio of 0.22 corresponds to a rather low v_P/v_S ratio of 1.67 observed in the area and typical for geothermal regions (Vavryčuk & Hrubcová, 2017).

Figure 9 shows the Coulomb stress change due to the slip produced by the 2008 and 2011 swarm earthquakes on the two fault segments. The stress change is calculated alternatively for three differently oriented fault planes activated during the 2014 sequence (Figure 6c). The two planes (connected with the strike-slip and oblique normal focal mechanisms) have been active in the 2008 and 2011 swarms; the third plane (connected with the reverse focal mechanism) was activated just in the 2014 sequence. Figures 9a and 9b indicate that the fault steps have a tendency to be further extended because the area of the positive Coulomb stress change (red area) touches the tips of the faults and samples the unfractured area with strike similar to that of the faults. However, the area between the fault tips is characterized by a large negative Coulomb stress change preventing activation of strike slips or normal events between the faults. By contrast, the Coulomb stress change calculated on the reverse fault activated in the 2014 sequence is strongly positive in the area just between the tips of the fault steps where the faults interact (Figure 9c).

Hence, the stress modeling proved that earthquakes with all three types of the focal mechanisms (strike slips, normal, and reverse) are plausible in the 2014 sequence but having different locations: the strike slips and normal events located at the fault tips, and the reverse focal mechanisms are optimum for earthquakes located in the stress anomaly between the fault tips.

In addition, a detailed image of the Coulomb stress change for optimally oriented faults and the rotation of the principal stress axes in the area around the fault tips are presented in Figure 10. The stress axes correspond to the complete stress field obtained by summing the regional background stress and the static stress produced by the 2008 and 2011 seismic activities. The figure documents that the orientations of the σ_2 and σ_3 axes change rapidly due to the fault interaction. This is visible, in particular, on the variation of the σ_3 axis (green lines at individual cells). This axis has a uniform azimuth of 220° outside the stress anomaly, but it significantly rotates inside the anomaly. The σ_2 and σ_3 axes even interchange their orientations between the fault tips when compared with those in the surrounding area. This nicely coincides with the stress variation detected by observations (see Figure 8c, right-hand panel).

Figure 10 also evidences how complicated the stress inversion of focal mechanisms in the area close to the fault tips is. Even though the target area is quite small with size of about 300 × 300 m, inverting for an overall stress using all types of focal mechanisms of earthquakes located at this area will yield incorrect results, because the stress field is strongly heterogeneous. This confirms the correctness of our

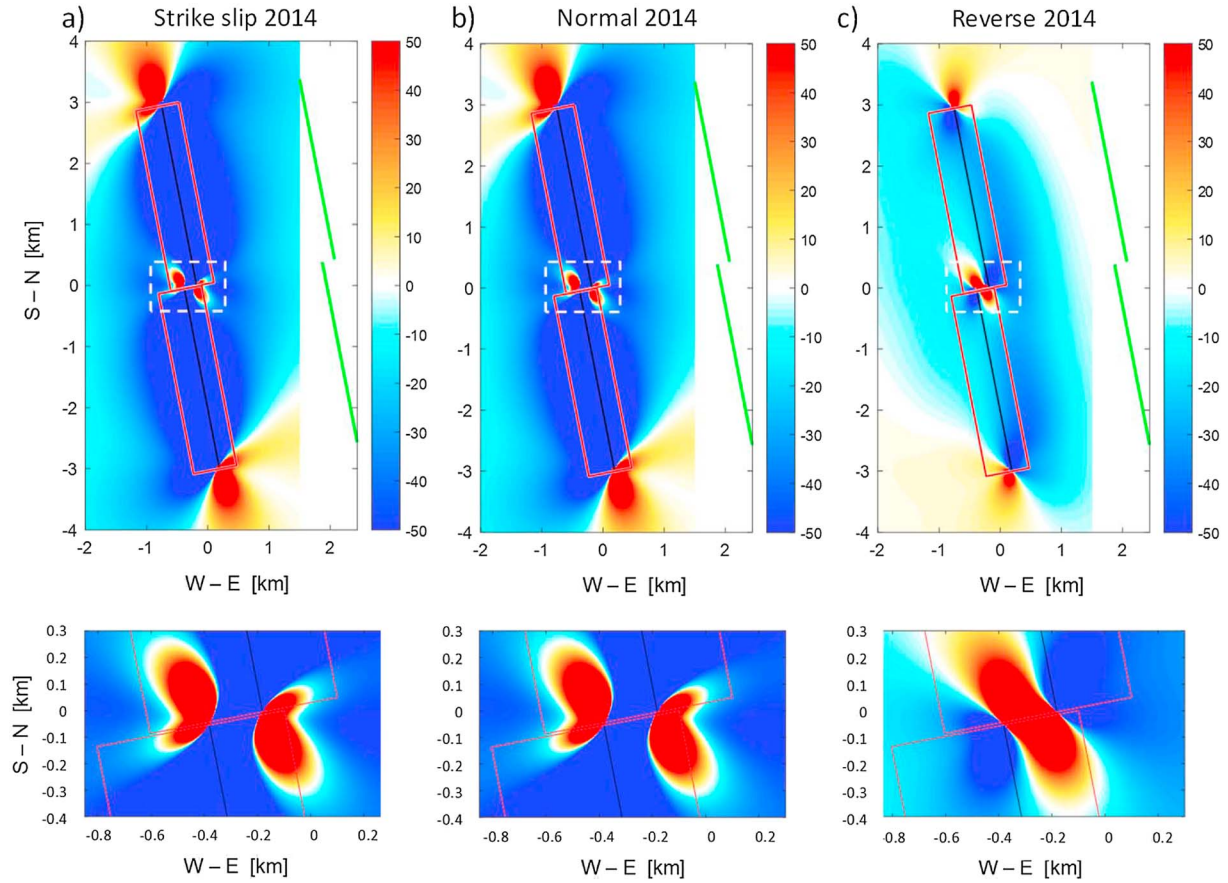

Figure 9. Modeling of the Coulomb stress change for the 2014 seismic sequence. The receiver fault is (a) the strike slip with the orientation identical with the fault steps, (b) the oblique normal fault conjugate to the fault steps, and (c) the reverse fault linking the individual fault segments. The area in the rectangles marked by the white dashed lines is shown in a zoomed view on bottom panels. The red lines delineate the margins of the fault steps in depth. The green lines denote the intersection of the fault steps with the Earth's surface. The Coulomb stress change is color coded and scaled in bars. Since the stress changes close to the fault tips are quite high due to the static stress change instability, they are clipped to the maximum value of the scale.

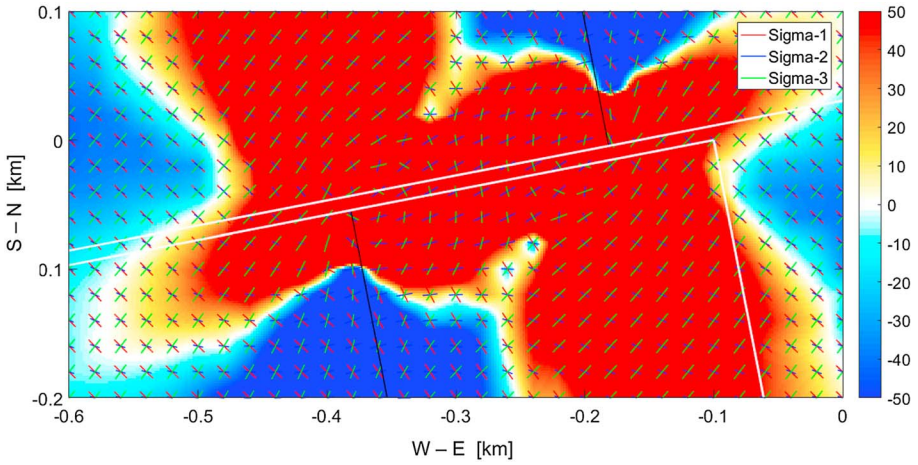

Figure 10. Modeling of the Coulomb stress change and of the orientation of the stress axes in the area between the fault tips. The white lines delineate the margins of the fault steps in depth. The directions of the principal stress axes σ_1 (red lines), σ_2 (blue lines), and σ_3 (green lines) are shown in cells with the size of 20 × 20 m. The Coulomb stress change is color coded and scaled in bars. Since the stress changes between to the fault tips are quite high being comparable to the background stress, they are clipped to the maximum value of the scale.

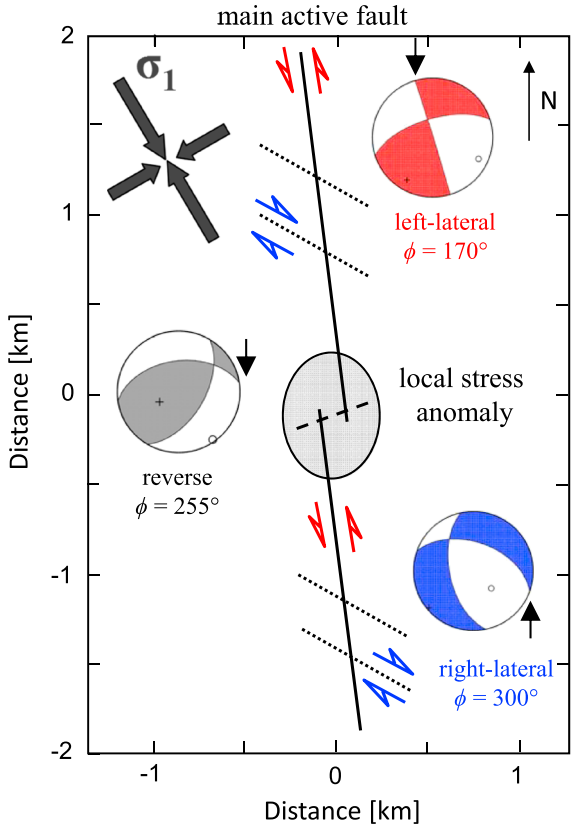

Figure 11. Tectonic sketch of the focal zone. The figure shows the fault steps (solid lines), the conjugate segments (dotted lines), and the newly formed fault (dashed line). The full black arrows show the orientation of the maximum and minimum compressive stress axes of the regional background stress. The beach balls show the focal mechanisms associated with the fault steps (in red), with the conjugate segments (in blue) and with the fault formed or activated within the stress anomaly (in gray). The faults outside the stress anomaly are weak due to a long-term fluid-driven erosion. By contrast, the fault inside the stress anomaly is of high strength. The black arrows in beach balls identify the faults. The area of the stress anomaly is shaded.

strategy when we inverted the reversed focal mechanisms related to the stress anomaly located between the fault tips separately (see Figure 8, right-hand column).

6. Discussion

The mainshock of the 2014 seismic sequence in West Bohemia with magnitude of 4.2 and the other two strongest earthquakes with magnitudes of 3.6 and 3.5 have focal mechanisms incompatible with the background tectonic stress in the region. This finding has already been reported by Hainzl et al. (2016) who studied the statistical properties of the 2014 activity in relation with the presence of fluids in the focal zone. The authors speculated that the unfavorably oriented mainshock in the 2014 sequence was most likely activated by high fluid pressure. The mainshock opened fluid pathways from a fluid source, and the subsequent migration of fluids caused an unusually fast rate of aftershocks. We argue, however, that the strongest earthquakes in 2014 with unfavorably oriented focal mechanisms could not be triggered by overpressurized fluids, because high pore pressure would activate existing and previously active favorably oriented faults rather than inactive unfavorably oriented ones. Therefore, the origin of the earthquakes with anomalous focal mechanisms should be different.

The strongest earthquakes of the 2014 sequence are located in the area of the fault interaction of two parallel fault segments (Figure 11). Both fault segments were activated in 2008 and 2011. The intense seismic activity in 2008 and 2011 accompanied probably also by an aseismic slip on the faults afterward created a local compressive stress anomaly leading finally to breaking the strength barrier between the faults. The mainshock and a portion of aftershocks displayed a reverse focal mechanism and occurred on a fracture that linked the existing fault steps. This interpretation is supported by (1) the orientation of the fault calculated from the focal mechanism of the mainshock, (2) distinctly different statistical properties of the 2014 sequence with extremely fast aftershock decay suggesting a formation of a high-strength fracture under compressive stress regime, (3) swapping of the σ_2 and σ_3 axes in the area between the tips of the interacting faults, and (4) the modeling of the Coulomb stress change of two parallel compressive fault steps that confirmed a high probability of the occurrence of reverse focal mechanisms and a rotation of stress axes between the fault tips.

Note that differences in the decay of aftershocks in time were studied by Valerio et al. (2017) for various seismogenic regions. The authors report that regions with compressive stress regimes, producing earthquakes with reverse focal mechanisms, are characterized by a remarkably faster energy release than areas with extensional stresses. Our observations coincide with these results and indicate that the fast energy release in the 2014 sequence can be due to the compressive stress in the focal zone. The slower energy release in the 2008 and 2011 sequences can originate in the strike-slip stress regime in the focal zone consistent with the regional background stress.

In addition, a compressive stress anomaly produced by the fault steps can explain the occurrence of the mainshock-aftershock character of the 2014 sequence. Fluid-rich geothermal regions are usually characterized by high heat flow with elevated temperatures and with mixed brittle-ductile failures manifested by the occurrence of a swarm-like seismicity (Ben-Zion & Lyakhovsky, 2006; Zaliapin & Ben-Zion, 2013). Accordingly, a long-term erosion of faults in West Bohemia by fluids caused probably their weakness with absence of strong asperities and produced repeating occurrence of earthquake swarms as documented by Vavryčuk and Hrubcová (2017) by analysis of non-DC components of seismic moment tensors. However, an interaction of the fault tips altered physical conditions in the focal zone. It changed locally the orientation of

stress and initiated forming or activating high-strength fractures that broke a barrier between the fault tips and linked the existing faults. Because of a compressive character of the stress anomaly, the involvement of fluids was minimized. Hence, the energy release on the high-strength fractures resembles the standard earthquake sequences being thus essentially different from the typical fluid-driven activity on existing active weak faults in the region.

Breaking a barrier between the tips of the previously active isolated faults and linking them during the 2014 activity increased the seismic hazard in the area. The strongest instrumentally recorded earthquake during the last 40 years occurred on the southern fault segment during the 1985/1986 earthquake swarm and reached magnitude M_L of 4.6. The area of the southern segment activated during the 1985/1986 swarm (Vavryčuk, 1993) was similar to that activated during the 2008 swarm with size of about 3 × 3 km (see Figure 2). An earthquake associated with rupturing the whole southern segment would reach magnitude M_w of about 5.0 (Wells & Coppersmith, 1994). The northern fault segment activated in the 2011 swarm is characterized by the same size of about 3 × 3 km as the northern fault segment (see Figure 2), and the maximum expected magnitude M_w is again about 5.0. However, if an earthquake ruptures the whole linked fault system, the magnitude M_w will increase to 5.4.

7. Conclusions

A detailed study of focal mechanisms and stress in the focal zone in West Bohemia evidences that fault steps can concentrate a local stress anomaly significantly disturbing the background stress. Consequently, breaking the barrier between the fault steps can trigger a seismic sequence with the focal mechanism of the mainshock incompatible with the regional background stress. When the barrier is broken, a fracture linking the fault steps is formed or activated. The fracture process can continue along the existing individual weak faults well oriented for shearing under the regional background stress. Hence, the linkage of the compressive fault steps or rupture jump between the fault segments increases the probability of the occurrence of a large earthquake in the region. Therefore, searching for compressive fault steps in seismically active regions is important for evaluating properly the seismic hazard.

Local stress anomalies caused by geometrical irregularities (e.g., kinks, discontinuities due to fault steps) or heterogeneities in strength along faults or fault systems significantly complicate the reconstruction of stress field from focal mechanisms. Such anomalies can be quite small in size but still affecting focal mechanisms and the character of the seismic sequence. They can be identified by observing an exceptionally wide variety of accurately determined focal mechanisms or by detecting anomalous focal mechanisms inconsistent with the regional background stress in some part of the focal zone. The paper documents that inverting focal mechanisms of the strongest earthquakes of a seismic sequence does not necessarily yield the orientation of the regional background stress.

Observation of swarm-like and mainshock-aftershock activities in one focal zone points out complex nature of rupture processes. In fluid-rich geothermal regions, characterized by high heat flow and intense rock-fluid interactions, the seismicity is typically associated with weak faults that produce a swarm-like seismicity. However, a local stress anomaly created by interaction of active weak faults can form or activate high-strength fault rupturing of which produces the mainshock-aftershock sequences. Hence, stress and strength heterogeneities in the focal zone are the key factors controlling extremely variable space-time evolution of seismic energy release.

Acknowledgments
We thank the Associate Editor J. Bruce H. Shyu, the three anonymous reviewers for their helpful comments, and Alena Boušková, Jana Doubravová, Josef Horálek, and Hana Jakoubková for their help in the preprocessing of the WEBNET data. The study was supported by the Grant Agency of the Czech Republic, grant 16-19751J. Seismic moment tensors of the 2008, 2011, and 2014 seismic sequences used for the stress analysis in this paper are available as the supporting information.

References

Adda-Bedia, M., & Madariaga, R. (2008). Seismic radiation from a kink on an antiplane fault. *Bulletin of the Seismological Society of America*, *98*(5), 2291–2302. https://doi.org/10.1785/0120080003

An, L. J. (1997). Maximum link distance between strike-slip faults: Observations and constraints. *Pure and Applied Geophysics*, *150*(1), 19–36. https://doi.org/10.1007/s000240050061

Arrias, R., Madariaga, R., & Adda-Bedia, M. (2011). Singular elasto-static field near a fault kink. *Pure and Applied Geophysics*, *168*(12), 2167–2179. https://doi.org/10.1007/s00024-011-0298-y

Bankwitz, P., Schneider, G., Kämpf, H., & Bankwitz, E. (2003). Structural characteristics of epicentral areas in Central Europe: Study case Cheb Basin (Czech Republic). *Journal of Geodynamics*, *35*(1-2), 5–32. https://doi.org/10.1016/S0264-3707(02)00051-0

Ben-Zion, Y., & Lyakhovsky, V. (2006). Analysis of aftershocks in a lithospheric model with seismogenic zone governed by damage rheology. *Geophysical Journal International*, *165*(1), 197–210. https://doi.org/10.1111/j.1365-246X.2006.02878.x

Bouchaala, F., Vavryčuk, V., & Fischer, T. (2013). Accuracy of the master-event and double-difference locations: Synthetic tests and application to seismicity in West Bohemia, Czech Republic. *Journal of Seismology*, *17*(3), 841–859. https://doi.org/10.1007/s10950-013-9357-4

Braeuer, K., Kaempf, H., Niedermann, S., & Strauch, G. (2018). Monitoring of helium and carbon isotopes in the western Eger rift area (Czech Republic): Relationships with the 2014 seismic activity and indications for recent (2000–2016) magmatic unrest. *Chemical Geology*, *482*, 131–145. https://doi.org/10.1016/j.chemgeo.2018.02.017

Braeuer, K., Kaempf, H., & Strauch, G. (2009). Earthquake swarms in non-volcanic regions: What fluids have to say. *Geophysical Research Letters*, *36*, L17309. https://doi.org/10.1029/2009GL039615

Čermáková, H., & Horálek, J. (2015). The 2011 West Bohemia (Central Europe) earthquake swarm compared with the previous swarms of 2000 and 2008. *Journal of Seismology*, *19*(4), 899–913. https://doi.org/10.1007/s10950-015-9502-3

Crider, J. G., & Pollard, D. D. (1998). Fault linkage: Three-dimensional mechanical interaction between echelon normal faults. *Journal of Geophysical Research*, *103*(B10), 24,373–24,391. https://doi.org/10.1029/98JB01353

Davi, R., & Vavryčuk, V. (2012). Seismic network calibration for retrieving accurate moment tensors. *Bulletin of the Seismological Society of America*, *102*(6), 2491–2506. https://doi.org/10.1785/0120110344

Fan, W., & Shearer, P. M. (2016). Fault interactions and triggering during the 10 January 2012 M_w 7.2 Sumatra earthquake. *Geophysical Research Letters*, *43*, 1934–1942. https://doi.org/10.1002/2016GL067785

Fischer, T., Horálek, J., Hrubcová, P., Vavryčuk, V., Bräuer, K., & Kämpf, H. (2014). Intra-continental earthquake swarms in West-Bohemia and Vogtland: A review. *Tectonophysics*, *611*, 1–27. https://doi.org/10.1016/j.tecto.2013.11.001

Fischer, T., Horálek, J., Michálek, J., & Bouškova, A. (2010). The 2008 West Bohemia earthquake swarm in the light of the WEBNET network. *Journal of Seismology*, *14*(4), 665–682. https://doi.org/10.1007/s10950-010-9189-4

Fossen, H., & Rotevatn, A. (2016). Fault linkage and relay structures in extensional settings—A review. *Earth-Science Reviews*, *154*, 14–28. https://doi.org/10.1016/j.earscirev.2015.11.014

Gupta, A., & Scholz, C. H. (2000). A model of normal fault interaction based on observations and theory. *Journal of Structural Geology*, *22*(7), 865–879. https://doi.org/10.1016/S0191-8141(00)00011-0

Hainzl, S., Fischer, T., Čermáková, H., Bachura, M., & Vlček, J. (2016). Aftershocks triggered by fluid intrusion: Evidence for the aftershock sequence occurred 2014 in West Bohemia/Vogtland. *Journal of Geophysical Research: Solid Earth*, *121*, 2575–2590. https://doi.org/10.1002/2015JB012582

Harris, R. A., & Day, S. M. (1993). Dynamics of fault interaction: Parallel strike-slip faults. *Journal of Geophysical Research*, *98*(B3), 4461–4472. https://doi.org/10.1029/92JB02272

Harris, R. A., & Day, S. M. (1999). Dynamic 3D simulations of earthquakes on en echelon faults. *Geophysical Research Letters*, *26*(14), 2089–2092. https://doi.org/10.1029/1999GL900377

Hasegawa, A., Yoshida, K., Asano, Y., Okada, T., Iinuma, T., & Ito, Y. (2012). Change in stress field after the 2011 great Tohoku-Oki earthquake. *Earth and Planetary Science Letters*, *355–356*, 231–243.

Hrubcová, P., Geissler, W. H., Bräuer, K., Vavryčuk, V., Tomek, Č., & Kämpf, H. (2017). Active magmatic underplating in western Eger rift, central Europe. *Tectonics*, *36*, 2846–2862. https://doi.org/10.1002/2017TC004710

Jakoubková, H., Horálek, J., & Fischer, T. (2017). 2014 mainshock-aftershock activity versus earthquake swarms in West Bohemia, Czech Republic. *Pure and Applied Geophysics*, *175*(1), 109–131. https://doi.org/10.1007/s00024-017-1679-7

Kaempf, H., Braeuer, K., Schumann, J., Hahne, K., & Strauch, G. (2013). CO2 discharge in an active, non-volcanic continental rift area (Czech Republic): Characterisation (delta C-13, He-3/He-4) and quantification of diffuse and vent CO_2 emissions. *Chemical Geology*, *339*, 71–83. https://doi.org/10.1016/j.chemgeo.2012.08.005

Kim, Y.-S., Peacock, D. C. P., & Sanderson, D. J. (2004). Fault damage zones. *Journal of Structural Geology*, *26*, 503–517.

Lin, J., & Stein, R. S. (2004). Stress triggering in thrust and subduction earthquakes and stress interaction between the southern San Andreas and nearby thrust and strike-slip faults. *Journal of Geophysical Research*, *109*, B02303. https://doi.org/10.1029/2003JB002607

Madariaga, R., Ampuero, J. P., & Adda-Bedia, M. (2006). Seismic radiation from simple models of earthquakes. In *Earthquakes: Radiated energy and the physics of faulting*, *Geophysical Monograph Series* (Vol. 170, pp. 223–236).

Madden, E. H., Maerten, F., & Pollard, D. D. (2013). Mechanics of nonplanar faults at extensional steps with application to the 1992 M 7.3 Landers, California, earthquake. *Journal of Geophysical Research: Solid Earth*, *118*, 3249–3263. https://doi.org/10.1002/jgrb.50237

Mansfeld, C., & Cartwright, J. (2001). Fault growth by linkage: Observations and implications from analogue models. *Journal of Structural Geology*, *23*(5), 745–763. https://doi.org/10.1016/S0191-8141(00)00134-6

Martínez-Garzón, P., Vavryčuk, V., Kwiatek, G., & Bohnhoff, M. (2016). Sensitivity of stress inversion of focal mechanisms to pore pressure changes. *Geophysical Research Letters*, *43*, 8441–8450. https://doi.org/10.1002/2016GL070145

Marzocchi, W., & Melini, D. (2014). On the earthquake predictability of fault interaction models. *Geophysical Research Letters*, *41*, 8294–8300. https://doi.org/10.1002/2014GL061718

Michael, A. J. (1984). Determination of stress from slip data: Faults and folds. *Journal of Geophysical Research*, *89*(B13), 11,517–11,526. https://doi.org/10.1029/JB089iB13p11517

Michael, A. J. (1987). Use of focal mechanisms to determine stress: A control study. *Journal of Geophysical Research*, *92*(B1), 357–368. https://doi.org/10.1029/JB092iB01p00357

Micklethwaite, S., Ford, A., Witt, W., & Sheldon, H. A. (2015). The where and how of faults, fluids and permeability—Insights from fault stepovers, scaling properties and gold mineralization. *Geofluids*, *15*(1-2), 240–251. https://doi.org/10.1111/gfl.12102

Nevitt, J. M., & Pollard, D. D. (2017). Impacts of off-fault plasticity on fault slip and interaction at the base of the seismogenic zone. *Geophysical Research Letters*, *44*, 1714–1723. https://doi.org/10.1002/2016GL071688

Oglesby, D. (2008). Rupture termination and jump on parallel offset faults. *Bulletin of the Seismological Society of America*, *98*(1), 440–447. https://doi.org/10.1785/0120070163

Okada, Y. (1992). Internal deformation due to shear and tensile faults in a half-space. *Bulletin of the Seismological Society of America*, *82*(2), 1018–1040.

Ryan, K. J., & Oglesby, D. D. (2014). Dynamically modeling fault step overs using various friction laws. *Journal of Geophysical Research: Solid Earth*, *119*, 5814–5829. https://doi.org/10.1002/2014JB011151

Sagong, M., & Bobet, A. (2002). Coalescence of multiple flaws in a rock-model material in uniaxial compression. *International Journal of Rock Mechanics and Mining Sciences*, *39*(2), 229–241. https://doi.org/10.1016/S1365-1609(02)00027-8

Špičák, A., & Lokajíček, T. (1986). Fault interaction and seismicity—Laboratory investigation and its seismotectonic interpretation. *Pure and Applied Geophysics*, *124*(4–5), 857–874. https://doi.org/10.1007/BF00879615

Toda, S., Stein, R. S., Richards-Dinger, K., & Bozkurt, S. B. (2005). Forecasting the evolution of seismicity in southern California: Animations built on earthquake stress transfer. *Journal of Geophysical Research*, *110*, B05S16. https://doi.org/10.1029/2004JB003415

Turner, R. C., Nadeau, R. M., & Bürgmann, R. (2013). Aseismic slip and fault interaction from repeating earthquakes in the Loma Prieta aftershock zone. *Geophysical Research Letters*, *40*, 1079–1083. https://doi.org/10.1002/grl.50212

Valerio, E., Tizzani, P., Carminati, E., & Doglioni, C. (2017). Longer aftershocks duration in extensional tectonic settings. *Scientific Reports*, *7*(1), 16403. https://doi.org/10.1038/s41598-017-14550-2

Vavryčuk, V. (1993). Crustal anisotropy from local observations of shear-wave splitting in West Bohemia, Czech Republic. *Bulletin of the Seismological Society of America*, *83*, 1420–1441.

Vavryčuk, V. (2002). Non-double-couple earthquakes of January 1997 in West Bohemia, Czech Republic: Evidence of tensile faulting. *Geophysical Journal International*, *149*(2), 364–373. https://doi.org/10.1046/j.1365-246X.2002.01654.x

Vavryčuk, V. (2011). Principal earthquakes: Theory and observations from the 2008 West Bohemia swarm. *Earth and Planetary Science Letters*, *305*(3-4), 290–296. https://doi.org/10.1016/j.epsl.2011.03.002

Vavryčuk, V. (2014). Iterative joint inversion for stress and fault orientations from focal mechanisms. *Geophysical Journal International*, *199*(1), 69–77. https://doi.org/10.1093/gji/ggu224

Vavryčuk, V., Adamová, P., Doubravová, J., & Jakoubková, H. (2017). Moment tensor inversion based on the principal component analysis of waveforms: Method and application to microearthquakes in West Bohemia, Czech Republic. *Seismological Research Letters*, *88*(5), 1303–1315. https://doi.org/10.1785/0220170027

Vavryčuk, V., Bouchaala, F., & Fischer, T. (2013). High-resolution fault image from accurate locations and focal mechanisms of the 2008 swarm earthquakes in West Bohemia, Czech Republic. *Tectonophysics*, *590*, 189–195. https://doi.org/10.1016/j.tecto.2013.01.025

Vavryčuk, V., & Hrubcová, P. (2017). Seismological evidence of fault weakening due to erosion by fluids from observations of intraplate earthquake swarms. *Journal of Geophysical Research: Solid Earth*, *122*, 3701–3718. https://doi.org/10.1002/2017JB013958

Wells, D. L., & Coppersmith, K. J. (1994). New empirical relationships among magnitude, rupture length, rupture width, rupture area and surface displacement. *Bulletin of the Seismological Society of America*, *84*(4), 974–1002.

Wesnousky, S. G. (2006). Predicting the endpoints of earthquake ruptures. *Nature*, *444*(7117), 358–360. https://doi.org/10.1038/nature05275

Yang, S.-Q., Jing, H.-W., Huang, Y.-H., Ranjith, P. G., & Jiao, Y.-Y. (2014). Fracture mechanical behavior of red sandstone containing a single fissure and two parallel fissures after exposure to different high temperature treatments. *Journal of Structural Geology*, *69*, 245–264. https://doi.org/10.1016/j.jsg.2014.10.014

Yoshida, K., Hasegawa, A., & Okada, T. (2015). Spatially heterogeneous stress field in the source area of the 2011 M_w 6.6 Fukushima-Hamadori earthquake, NE Japan, probably caused by static stress change. *Geophysical Journal International*, *201*(2), 1062–1071. https://doi.org/10.1093/gji/ggv068

Yoshida, K., Hasegawa, A., Okada, T., & Iinuma, T. (2014). Changes in the stress field after the 2008 M7.2 Iwate-Miyagi Nairiku earthquake in northeastern Japan. *Journal of Geophysical Research: Solid Earth*, *119*, 9016–9030. https://doi.org/10.1002/2014JB011291

Yoshida, K., Hasegawa, A., Okada, T., Iinuma, T., Ito, Y., & Asano, Y. (2012). Stress before and after the 2011 great Tohoku-Oki earthquake and induced earthquakes in inland areas of eastern Japan. *Geophysical Research Letters*, *39*, L03302. https://doi.org/10.1029/2011GL049729

Zaliapin, I., & Ben-Zion, Y. (2013). Earthquake clusters in southern California II: Classification and relation to physical properties of the crust. *Journal of Geophysical Research: Solid Earth*, *118*, 2865–2877. https://doi.org/10.1002/jgrb.50178

Zuza, A. V., Yin, A., Lin, J., & Sun, M. (2017). Spacing and strength of active continental strike-slip faults. *Earth and Planetary Science Letters*, *457*, 49–62. https://doi.org/10.1016/j.epsl.2016.09.041